Journal of Porous Materials (2018) 25:1649–1658
https://doi.org/10.1007/s10934-018-0578-3

Enhanced catalytic oxidation of monoterpenes by zeolite-Y entrapped iron complex: spectral studies and mechanistic vision

Jignasu P. Mehta[1] · Digvijaysinh K. Parmar[1] · Haresh D. Nakum[1] · Dinesh R. Godhani[1] · Nisheeth C. Desai[1]

Published online: 9 February 2018

Abstract
$[Fe(L)_2(H_2O)_2]$–Y complex (where, L = (*Z*)-2-((4-hydroxybenzylidene)-amino)benzoic acid) has been synthesized by Flexible Ligand (FL) method and characterized by chemical analysis (CHN, ICP-OES, TGA, AAS), diffraction method (XRD), absorption spectroscopy (FTIR, UV–Vis), BET and SEM techniques. To investigate the catalytic performance (activity, stability, and reusability), $[Fe(L)_2(H_2O)_2]$–Y was employed as heterogeneous catalyst in the liquid phase oxidation of α-pinene and limonene with H_2O_2 oxidant. $[Fe(L)_2(H_2O)_2]$–Y catalyzed the oxidation of α-pinene via free radical formation as confirmed by in-situ IR and DR UV–Vis spectroscopy. $[Fe(L)_2(H_2O)_2]$–Y showed conversion of α-pinene (67%) and limonene (79%) with better TONs, which is far better performance than neat iron complex.

Keywords Metal complex · Zeolite-Y · Heterogeneous catalysis · Oxidation · Monoterpenes

1 Introduction

Oxyfunctionalized derivatives of monoterpenes are key raw materials of great importance as they used in the perfumery, aromatherapy and herbal remedies owing to their pleasant fragrance [1–3]. Increasingly strict environmental regulations have compelled the modification of a number of chemical processes including the oxidation of monoterpenes which improved number of times from the usage of homogeneous systems viz., mineral acids, transition metals, and metal complexes [4, 5] to eco-friendly heterogeneous systems viz., mixed metal oxides [6, 7], supported Ionic Liquid catalyst [8], biocatalytic epoxidation [9], zeolite-Y entrapped complexes [10–12], MCM-41 [13], SBA-15 [14], and polymer supported catalyst [15].

In particular, zeolite-Y hold the exchangeable sodium cations which allow the introduction of different metal ions. Moreover, due to the porous structure, zeolite-Y can act as "host materials" for incoming guest molecules which make them interesting and valuable for heterogeneous catalysis. In contrast to homogeneous systems, the metal complexes entrapped within a zeolite-Y, providing unlimited structural and chemical variations [16] through electrostatic, [17–19] covalent, [20] and dative [21] binding, which is nothing but an alternate way for the heterogenization, with additional advantages viz., easy separation, shape selectivity, site isolation, and thermal stability [22–24]. The metal complex, once formed inside the cavity, does not diffuse out and pass in the liquid phase during the catalytic reaction. The heterogeneously catalyzed oxidation of monoterpenes [10–12] gave a remarkably superior TONs and therefore much increased conversion to oxyfunctionalized derivatives as compared to their homogeneous counterparts.

Our group is principally engaged to identify the nature of zeolite-Y entrapped metal complexes on selective oxidation reactions [25–27]. Herein we report the catalytic acts of zeolite-Y entrapped iron complex in the liquid phase oxidation of monoterpenes using 30% H_2O_2 as an oxidant.

2 Materials and methods

All chemicals used in this work are of AR grade and are used as received from Aldrich. The elemental analysis of the synthesized materials was carried out on Perkin Elmer, USA 2400-II CHN analyzer. The content of Na(I), Al(III), Si(IV) and Fe(II) ions were determined by ICP-OES using

✉ Jignasu P. Mehta
jpm1569@yahoo.co.in

[1] Department of Chemistry, (UGC NON-SAP & DST-FIST Sponsored Department), Mahatma Gandhi Campus, Maharaja Krishnakumarsinhji Bhavnagar University, Bhavnagar, Gujarat 364 002, India

Perkin Elmer optima 2000 DV model. TGA was carried out using Perkin Elmer equipment and with the heating rate of 10 K min^{-1} under a flow of dry air. The XRD patterns of the materials were recorded by a Bruker AXS D_8 Advance X-ray powder diffractometer with a CuKα radiation as the incident beam. FTIR spectra (4000–400 cm^{-1}) of materials were recorded on a Thermo Nicolet IR200 FT-IR spectrometer in KBr. Electronic spectra were recorded on a UV-1800 spectrophotometer, SHIMADZU using a quartz cell of 1 cm^3 optical path. The diffuse reflectance (DR) UV–Vis spectra of neat and entrapped Fe complexes were recorded on UV reflectance spectrometer (Model: LAMDA 19 UV/VIS/NIR) in the solid phase at room temperature. The specific surface areas and pore volumes were obtained from nitrogen adsorption–desorption isotherms measured by a multipoint BET method using ASAP 2010, micromeritics surface area analyser. The morphology of $[Fe(L)_2(H_2O)_2]$–Y material was checked before and after Soxhlet extraction by SEM instrument (Model: LEO 1430 VP). Reaction products were identified using GC-MS having a BP-5 capillary column (30 m × 0.25 mm × 0.25 µm) 95% silicoxane surface and FID detector.

2.1 Synthesis of ligand 'L'

Ligand 'L' ((*Z*)-2-((4-hydroxybenzylidene)amino)benzoic acid) was synthesized by condensation of 4-hydroxy benzaldehyde with 2-amino benzoic acid as reported earlier (Scheme 1) [28]. *Ligand* orange crystals; m.p. 226–228 °C; Anal. found (%) C(69.68), H(4.53), N(5.80); Calcd. (%), C(69.70), H(4.60), N(5.81). ^{1}H NMR, δ ppm: 7.141–8.109 (m, 8H, Ar–H); 8.810 (s, 1H, HC=N); 14.701 (s, 1H, Ar–OH); 15.247 (s, 1H, –COOH), ^{13}C NMR: 103.403–133.585 (11C, Ar–C); 151.418 (1C, ≡C–OH); 157.405 (1C, –C=N–); 170.218 (1C, –COOH).

2.2 Synthesis of neat iron complex

An aqueous solution of 10 mmol $FeSO_4 \cdot 7H_2O$ was added to an methanolic solution of 20 mmol ligand L with constant stirring, and the resulting solution was refluxed at 80 °C for 4–5 h. Sodium acetate was added to adjust the pH of the solution around 5–6. The complex was separated by filtration and dried (Scheme 1).

2.3 Synthesis of zeolite-Y entrapped iron complex $[Fe(L)_2(H_2O)_2]$–Y

To prepare the zeolite-Y entrapped iron complex via FL method (Scheme 2), sodium ions of zeolite-Y were replaced by Fe(II) ions through ion exchange method as reported earlier [29]. Further, Fe(II)–Y was added to ligand L suspended in boiling 1,4-dioxane with constant stirring and was refluxed for 12 h. Here, the ligand enters into the cavity of zeolite-Y because of their flexible nature and interact with the previously exchanged iron metal ion. The product thus obtained was filtered, soxhlet extracted, washed, and dried in an oven at 120 °C overnight under reduced pressure [25]. The resulted material is hereinafter designated as $[Fe(L)_2(H_2O)_2]$–Y.

2.4 Catalytic oxidation of monoterpenes

The reactions were carried out by using α-pinene and limonene as typical substrates, and H_2O_2 as an oxidant with the appropriate amount of catalyst in acetonitrile solvent. The liquid organic products were analyzed by using a gas chromatography and were identified by comparison with authentic samples (Scheme 3).

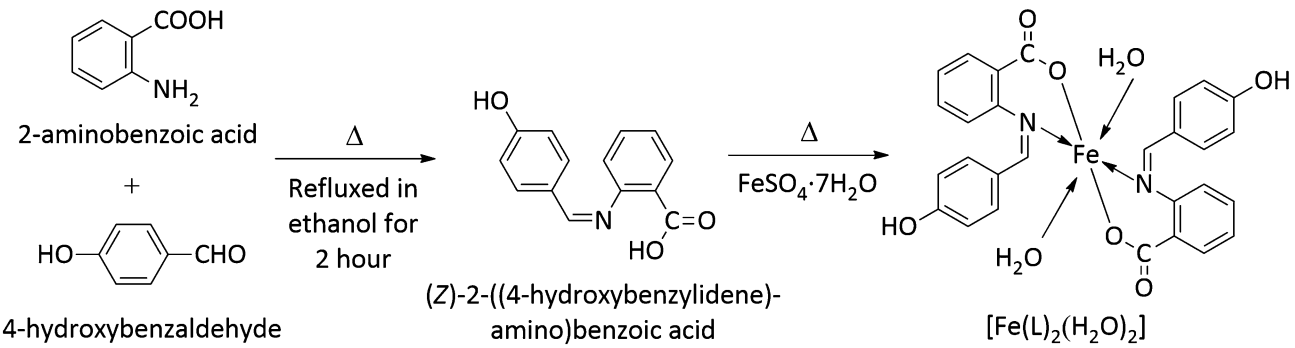

Scheme 1 Synthesis of Schiff base ligand and neat iron complex

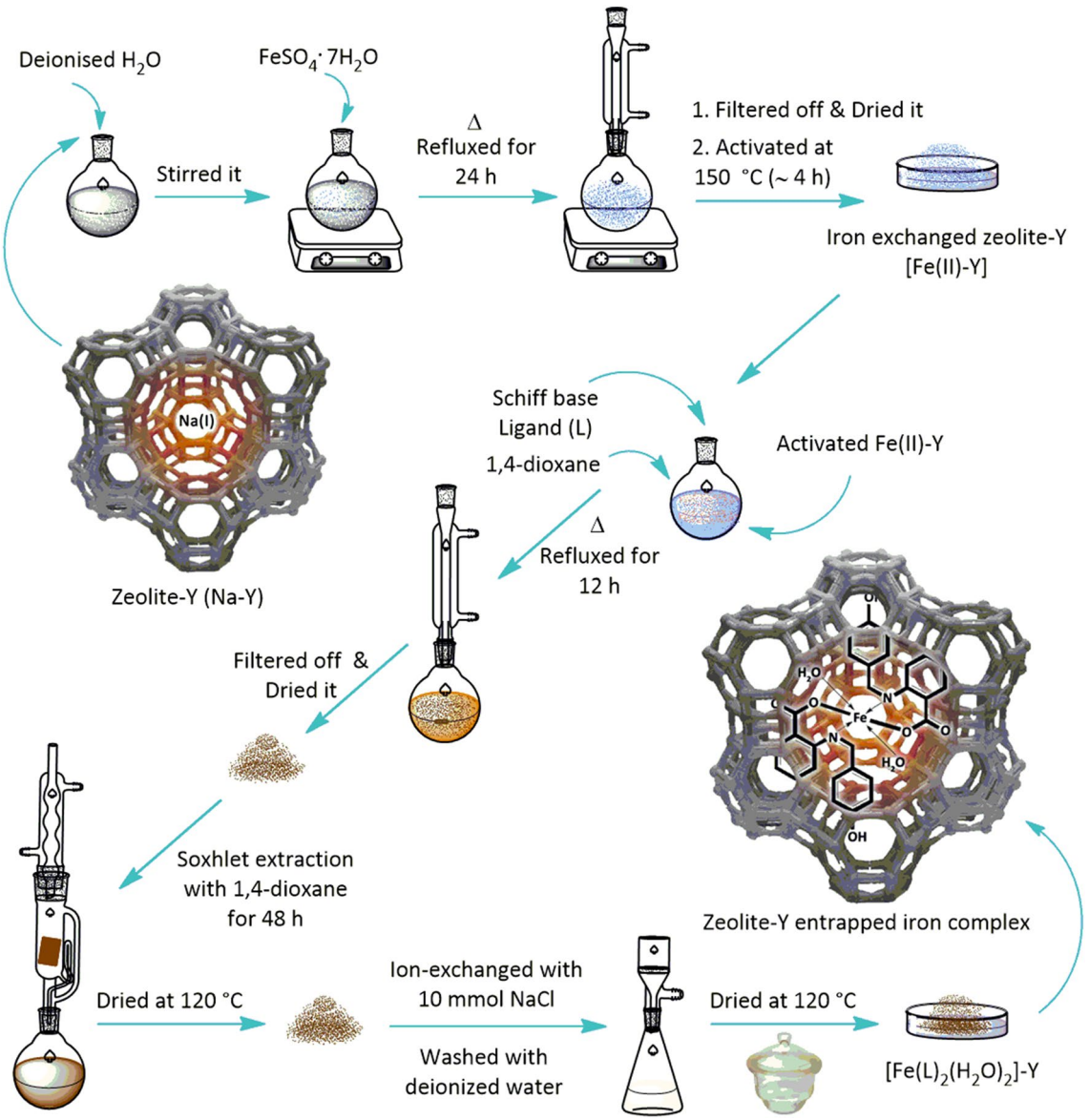

Scheme 2 Synthetic path for the entrapment of iron complex inside the nanopores of zeolite-Y

3 Results and discussion

3.1 Elemental analysis

The unaffected Si/Al ratio in both the Fe(II)–Y and $[Fe(L)_2(H_2O)_2]$–Y with that of the parent Na–Y (2.60) confirms the absence of de-alumination after metal ion exchange and entrapment of complex inside the nanopores as well (Table 1). Moreover, C/N ratio in the entrapped complex has been found similar with that of the respective neat complex, which confirms the presence of organic matter in the zeolite-Y [30].

3.2 BET surface area analysis

As per the data given in Table 2, the surface area and pore volume of zeolite-Y entrapped $[Fe(L)_2(H_2O)_2]$–Y complex reduced to ~ 40–50% as compared to Fe(II)–Y. The decrease amount is directed by the introduction of ligand, its expanse and the geometrical conformation with Fe(II) inside the zeolitic framework [31].

Scheme 3 The catalytic reaction of oxidation of α-pinene and limonene

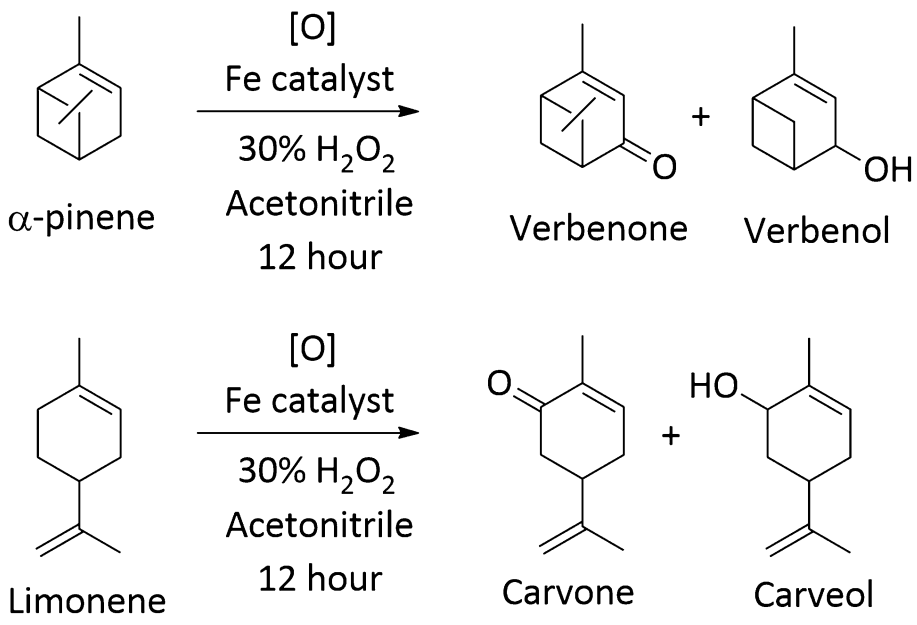

Table 1 Chemical composition data of synthesized materials

Materials	Elements found (%)							
	C	H	N	M	C/N	Si	Al	Si/Al
Na–Y	–	–	–	–	–	17.16	6.60	2.60
Fe(II)–Y	–	–	–	6.85	–	16.62	6.39	2.60
$[Fe(L)_2(H_2O)_2]\cdot 2H_2O$	55.40 (55.28)	4.53 (4.64)	4.62 (4.60)	9.01 (9.18)	11.99 (12.01)	–	–	–
$[Fe(L)_2(H_2O)_2]$–Y	2.53	0.28	0.21	0.93	12.04	15.35	5.90	2.60

% found (calculated)

Table 2 BET data of synthesized materials

Materials	BET surface area ($m^2\ g^{-1}$)	Microporous volume[a] ($cm^3\ g^{-1}$)
Na–Y	630	0.320
Fe(II)–Y	562	0.254
$[Fe(L)_2(H_2O)_2]$–Y	348	0.135

[a]From the N_2 adsorption isotherm at 77 K, calculated by the *BJH*-method

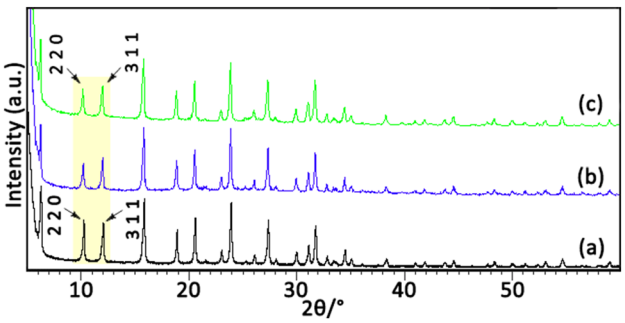

Fig. 1 XRD patterns of (*a*) Na–Y, (*b*) Fe(II)–Y, and (*c*) $[Fe(L)_2(H_2O)_2]$–Y

3.3 X-ray diffraction study

A minor alteration in peak intensity has been noticed in XRD patterns of zeolite-Y modified materials as shown in Fig. 1. For instance, the relationship $I_{220} > I_{311}$ was observed for zeolite-Y, but for the iron exchanged and entrapped iron complex it was reversed as $I_{311} > I_{220}$. This intensity alteration is due to the replacement of randomly distributed framework sodium ions in zeolite-Y by Fe(II) [32]. Apart from that, similar XRD patterns of modified zeolites with that of the parent zeolite-Y specifies the holding of the crystallinity of the zeolite-Y framework.

3.4 Scanning electron microscopy analysis

The morphological features of the entrapped complex $[Fe(L)_2(H_2O)_2]$–Y was obtained from the SEM studies. As seen from SEM images (Fig. 2a, b), there are some

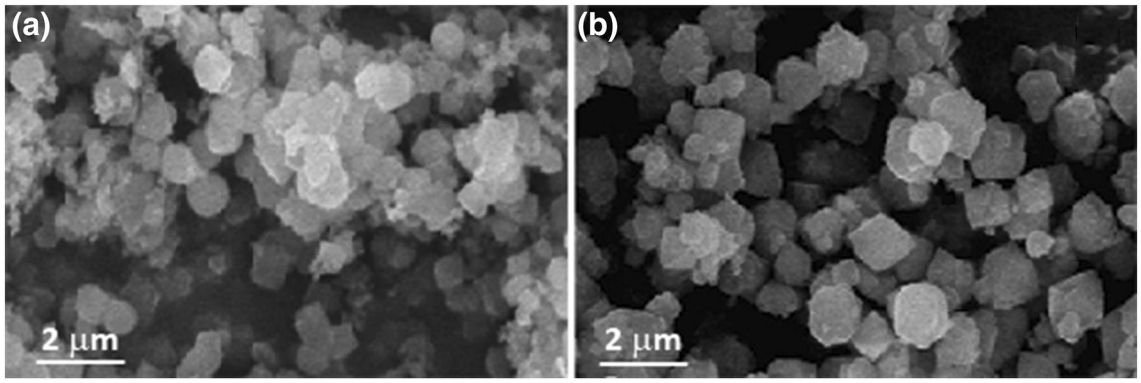

Fig. 2 SEM images of $[Fe(L)_2(H_2O)_2]$–Y **a** before and **b** after Soxhlet extraction

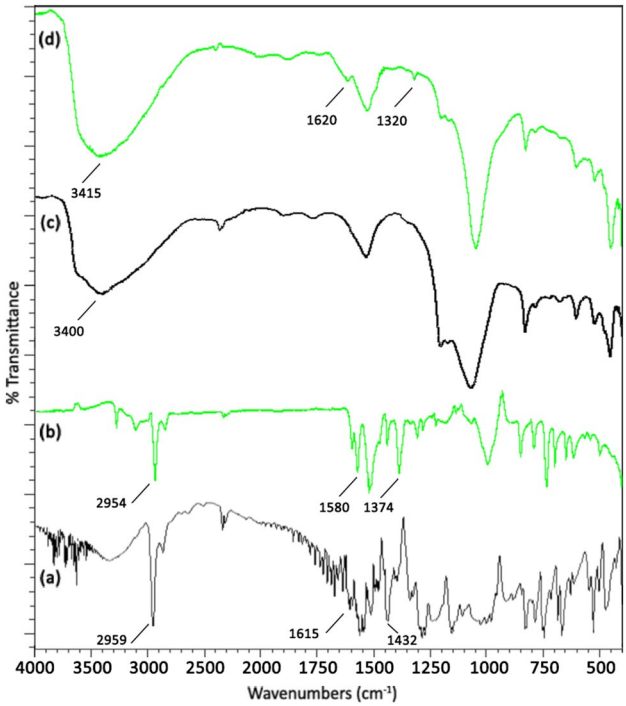

Fig. 3 FT-IR spectra of (*a*) L, (*b*) $[Fe(L)_2(H_2O)_2]\cdot 2H_2O$, (*c*) Na–Y, and (*d*) $[Fe(L)_2(H_2O)_2]$–Y

extraneous species on the surface of $[Fe(L)_2(H_2O)_2]$–Y before soxhlet extraction, however, the material surface after soxhlet extraction possess well distribution of particles [33], which confirms the complete removal of the deposited species after soxhlet extraction.

3.5 Fourier transform infrared (FTIR) spectroscopy

The IR spectral data of synthesized materials are shown in Fig. 3. IR spectra of the complexes exhibit $\nu_{(C=N)}$ vibrations of the azomethine group at 1580–1620 cm^{-1} and $\nu_{(C-O)}$ stretching vibrations of phenolate moiety at 1320–1375 cm^{-1} are significantly shifted as compared to the free ligand L, which is in good accordance with the published data [34–37], specifies the coordination of nitrogen and oxygen with metal in the free as well as entrapped state. However, the intensities of the $\nu_{(C-O)}$ and $\nu_{(C=N)}$ bands in the zeolite-Y entrapped complex are weak due to the low concentration of the complex inside zeolite-Y cavities. The broad bands detected at ~2900–3400 cm^{-1} are due to the hydroxyl group. These bands are not significantly altered in the entrapped complex.

3.6 UV–Vis spectroscopy

The electronic spectra of ligand L and neat complex were recorded in methanol, while of Na–Y and zeolite-Y entrapped complex were taken in dilute HF solution. As shown in Fig. 4, free ligand L exhibit three absorption bands at 259, 285, and 336 corresponding to ILCT, $\pi \rightarrow \pi^*$ (aromatic moiety) and $n \rightarrow \pi^*$ (C=N chromophore) transitions, respectively.

The electronic spectra of neat complex exhibit absorption in the region 220–310 nm, assigned to $\pi \rightarrow \pi^*$ transition occurs in the aromatic rings. The intense broad band at 336 nm assigned to the $t_2(M) \rightarrow \pi^*(L)$ CT transition. In addition, weak bands at 402 and 697 nm assigned to *d-d* transitions, suggesting an octahedral environment around the metal ion in Fe complex [38]. The spectra of entrapped complex show absorption bands at 447 and 538 nm attributed to *d–d* transition. This specifies the existence of complex inside the nanopores of zeolite-Y.

3.7 Thermogravimetric analysis

According to TGA data given in Table 3, the ligand L displays first mass loss of 41.3% in the range 140–160 °C, which may be recognized to the liberation of the first part of the ligand. In the second stage, remaining part loses within the temperature range 161–250 °C, with an

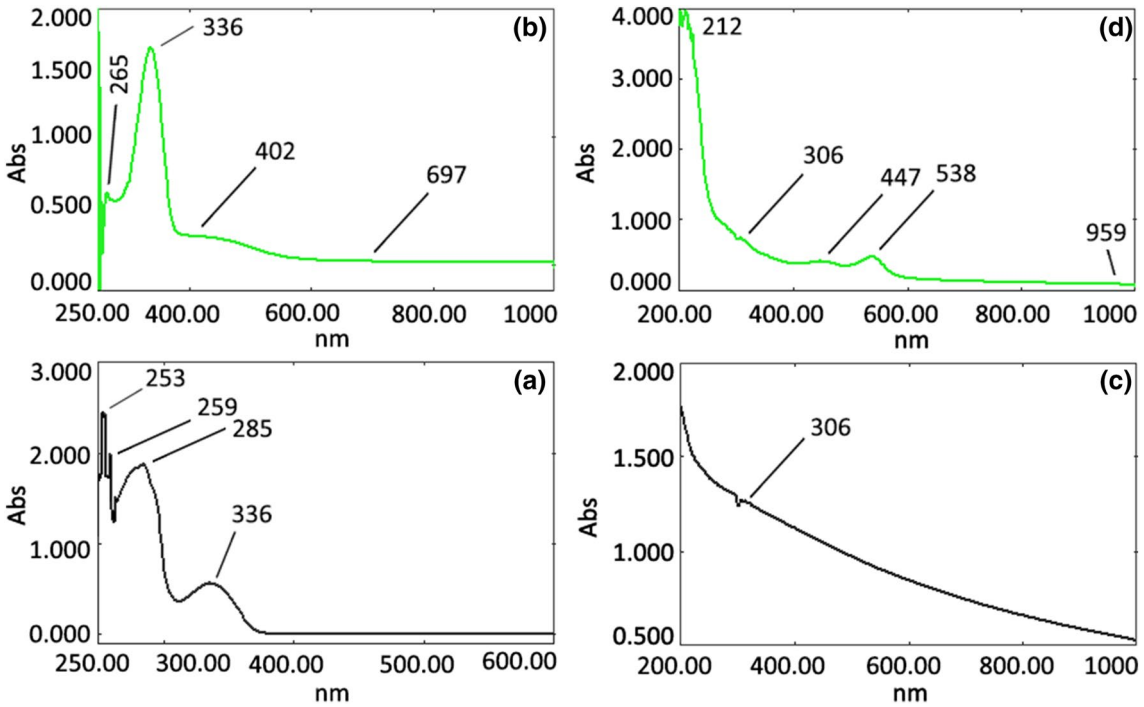

Fig. 4 Electronic spectra of **a** L, **b** $[Fe(L)_2(H_2O)_2]\cdot 2H_2O$, **c** Na–Y, and **d** $[Fe(L)_2(H_2O)_2]$–Y

Table 3 Thermogravimetric data of synthesized materials

Materials	Temperature range (°C)	Weight loss (%) (calc.)	Group loss (%)
L	140–160	41.3	Removal of $C_7H_6O_2-$ part
	161–250	57.8	Removal of $-C_8H_9NO$ part
$[Fe(L)_2(H_2O)_2]\cdot 2H_2O$	30–200	8.21 (10.29)	Crystallization + coordinated H_2O
	201–600	77.05 (82.51)	Ligand
	601–700	9.24 (8.00)	Fe_2O_3
$[Fe(L)_2(H_2O)_2]$–Y	50–200	6.80	Intrazeolite + coordinated H_2O
	451–700	8.34	Decomposition of complex

estimated mass loss of 57.8%. The TGA graph of neat complex involves two distinct weight losses. First part consists mass loss of ~ 10% which is due to the removal of crystallization and coordinated water molecules within temperature range of 30–200 °C. The second part is in the temperature range of 201–600 °C associated with the removal of ligand L with the observed mass loss of ~ 75%. The final residues were estimated as metal oxides. The TGA graph of entrapped complex consists two separate weight losses. The removal of intrazeolite and coordinated water molecules falls in the temperature range of 50–200 °C, followed by second part above 450 °C involves the weight loss of ~ 8% owing to the decomposition of metal complex. Based on the thermal analysis data, we may conclude that zeolite-Y entrapped Fe(II) complex may be treated thermally without any major decomposition [39].

3.8 Catalytic studies

The properties of four different catalytic systems have been discussed by taking Na–Y, Fe(II)–Y, $[Fe(L)_2(H_2O)_2]\cdot 2H_2O$, and $[Fe(L)_2(H_2O)_2]$–Y materials. The composition of the reaction medium was substrate (10 mmol), 20 mg of catalyst, and 3 mL of acetonitrile solvent (Table 4). Resulted mixture was heated at 80 °C with constant stirring, and the oxidant, 30% H_2O_2 (20 mmol) was progressively added to the reaction medium at a rate of 0.05 mL min^{-1} using a KD Scientific Syringe Pump: KDS 200P. The reaction products were analysed and identified as mentioned above.

As shown in Table 4, inability of parent zeolite-Y and metal exchanged Fe(II)–Y to carry out the oxidation proves that the metal complex is responsible for the substrate conversion and not the host or metal alone [40]. The catalytic activity of entrapped iron complex was found to be

Table 4 Efficiency of Na–Y, Fe(II)–Y, $[Fe(L)_2(H_2O)_2]\cdot 2H_2O$ and $[Fe(L)_2(H_2O)_2]$–Y catalysts over oxidation of monoterpenes and outcome of recovered catalyst

Entry	Substrate/catalyst	Na–Y		Fe(II)–Y		$[Fe(L)_2(H_2O)_2]\cdot 2H_2O$				$[Fe(L)_2(H_2O)_2]$–Y			
		Conversion (%)	Selectivity (%)	Conversion (%)	Selectivity (%)	Conversion (%)	TON[a]	TOF[b] (h^{-1})	Selectivity (%)	Conversion (%)	TON[a]	TOF[b] (h^{-1})	Selectivity (%)
1	α-Pinene	3	28[f] 41[g]	12	30[f] 54[g]	59	183	15	59[f] 14[g]	67	2012	168	64[f] 19[g]
2	α-Pinene[c]	–	–	–	–	–	–	–	–	64	1921	160	63[f] 19[g]
3	α-Pinene[d]	–	–	–	–	–	–	–	–	64	1921	160	64[f] 17[g]
4	α-Pinene[e]	–	–	–	–	–	–	–	–	63	1891	157	64[f] 17[g]
5	Limonene	3.8	51[h] 36[i]	14.3	42[h] 29[i]	66	205	17	63[h] 17[i]	79	2372	198	71[h] 14[i]

Reaction conditions: 10 mmol substrate, 20 mmol 30% H_2O_2, 20 mg catalyst, 3 mL acetonitrile, 80 °C, 12 h

[a]*TON* turnover number = mol of substrate converted/mol of metal

[b]*TOF* turnover frequency = mol of substrate converted/(mol of metal × hour)

[c]First

[d]Second

[e]Third recycled catalyst

[f]Verbenone

[g]Verbenol

[h]Carvone

[i]Carveol

better over the neat iron complex. As per the data given in Table 1, $[Fe(L)_2(H_2O)_2]$–Y offers the best result amongst all. α-pinene and limonene give major products verbenone and carvone, respectively.

An important feature to be considered in the liquid phase oxidation with solid catalysts is the stability of the catalyst, the possibility of catalyst recycling and the heterogeneity of the reaction. The stability of $[Fe(L)_2(H_2O)_2]$–Y was tested up to four cycles (fresh + three cycles) in the oxidation of α-pinene (Table 4, entry 2–4). The conversion of α-pinene decreased from 67 to 64% from fresh to first recycle. Further recyclability result shows almost similar conversion and selectivity from second to fourth cycles (~ 63% conversion at the end of the fourth cycle). Moreover, according to AAS analysis report, the absence of metal content in the liquid phase of the reaction mixture after completion of the reaction confirms the heterogeneity of the entrapped complex $[Fe(L)_2(H_2O)_2]$–Y.

In order to discover the catalytic cycle of α-pinene oxidation, the progress of the reaction has been observed using UV–Vis spectroscopy by treating the 10^{-3} M neat Fe(II) complex with H_2O_2 in methanolic solution (Fig. 5). The intensity of the bands closely at 697 and 340 nm was decreased. Though, the position of bands were remained unaffected. Further addition of H_2O_2 resulted in vanishing of *d–d* band. An isosbestic point observed at 290 nm specifies the conversion of Fe(II) to Fe(III), which clearly suggests a direct interaction of Fe center with H_2O_2.

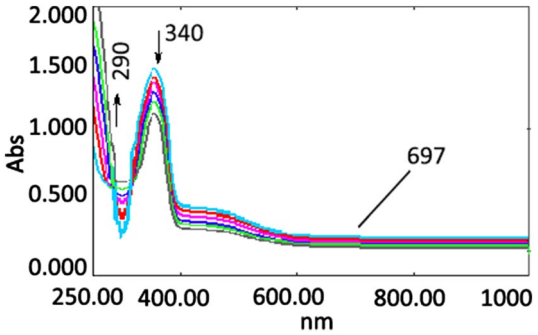

Fig. 5 UV–Vis spectra of $[Fe(L)_2(H_2O)_2]\cdot 2H_2O$ taken during consecutive addition of methanolic H_2O_2

As shown in Fig. 6, in-situ IR spectra of intermediate $[(H_2O)_2(L)_2Fe\text{-}OOH]\cdot H_2O$ of a separate reaction of hydrogen peroxide with neat Fe(II) complex was taken. According to spectra, strong band of $\upsilon_{(O-H)}$ compared to neat Fe(II) complex indicates the presence of –OH group in it. Based on these observations, it can be concluded that oxygen of Fe-OOH is transfer to the substrate via homolytic cleavage of peroxide bonds (–O–O–). Moreover, non-participation of Fe(III)–O–O–Fe(III) can be explained by the existence of $\upsilon_{(O-H)}$ broad band in the FTIR of intermediate.

The catalytic route for the oxidation of α-pinene by $[Fe(L)_2(H_2O)_2]$–Y is given in Scheme 3. The DR UV–Vis spectra (Fig. 7) of the zeolite-Y entrapped iron complex shows that charge transfer and *d–d* bands are mainly intensified and blue shifted which are closely associated with the metal centre indicate that the zeolite framework has a weighty effect on the structure of the complex. Therefore, upon entrapment, the in-plane ligand field becomes stronger, the axial ligands alongside being weaker, which may ease the dissociation of one axial H_2O molecule of hexacoordinated iron complex, which results in the formation of a vacant site on the metal ion, making coordinatively unsaturated (CN = 5) complex (**A**). The unoccupied site can be filled by incoming H_2O_2 to produce metal-peroxo species (**B**) [41]. Due to the weak bonding among the oxygen atoms, peroxide undergoes homolytic cleavage yielding highly reactive free radical (**C**). This cleavage is enhanced by temperature or chemical reactions. Free radical further reacts with α-pinene to form an intermediate species (**D**). Next step involves the formation of verbenol (**E**), which further reacts with free radical species (**C**) to form intermediate species (**F**), which eliminate water molecule to produce verbenone (**G**) (Scheme 4).

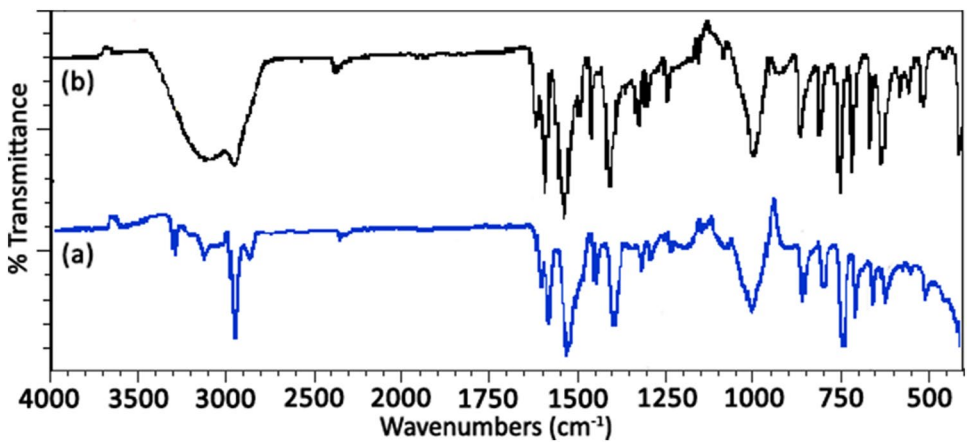

Fig. 6 (*a*) FT-IR spectra of $[Fe(L)_2(H_2O)_2]\cdot 2H_2O$, and (*b*) in-situ FT-IR spectra of intermediate $[(H2O)_2(L)2Fe\text{-}OOH]\cdot H_2O$

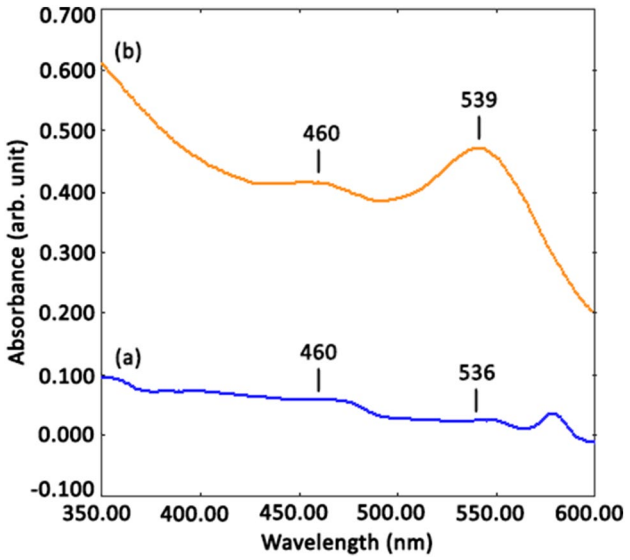

Fig. 7 DR UV–Vis spectra of (*a*) $[Fe(L)_2(H_2O)_2]\cdot 2H_2O$ and (*b*) $[Fe(L)_2(H_2O)_2]$–Y

4 Conclusions

In conclusion, $[Fe(L)_2(H_2O)_2]$–Y succeed to give 2012 TONs in α-pinene oxidation with 64% selectivity of the verbenone, while it oxidizes limonene to give 2372 TONs with 71% selectivity of the carvone. The observed catalytic behaviour, however a consequence of distorted structure adopted by the iron complex upon entrapment. As we have seen, to fit into the cavity, the complex undergone a distortion, which help us in change the catalytic efficiency of metal-centered active sites.

Moreover, the catalytic route of α-pinene oxidation by a catalyst $[Fe(L)_2(H_2O)_2]$–Y proceed via formation of metal-peroxo species followed by free radical generation which then react with substrate to give product. The reaction takes place inside the cavity of zeolite as substrate is small enough to diffuse through the micropores of and react with preloaded metal complex to give product which then easily diffuse out from the framework. To summarize, the use of the host matrix as a "catalytic interstellar" can switch

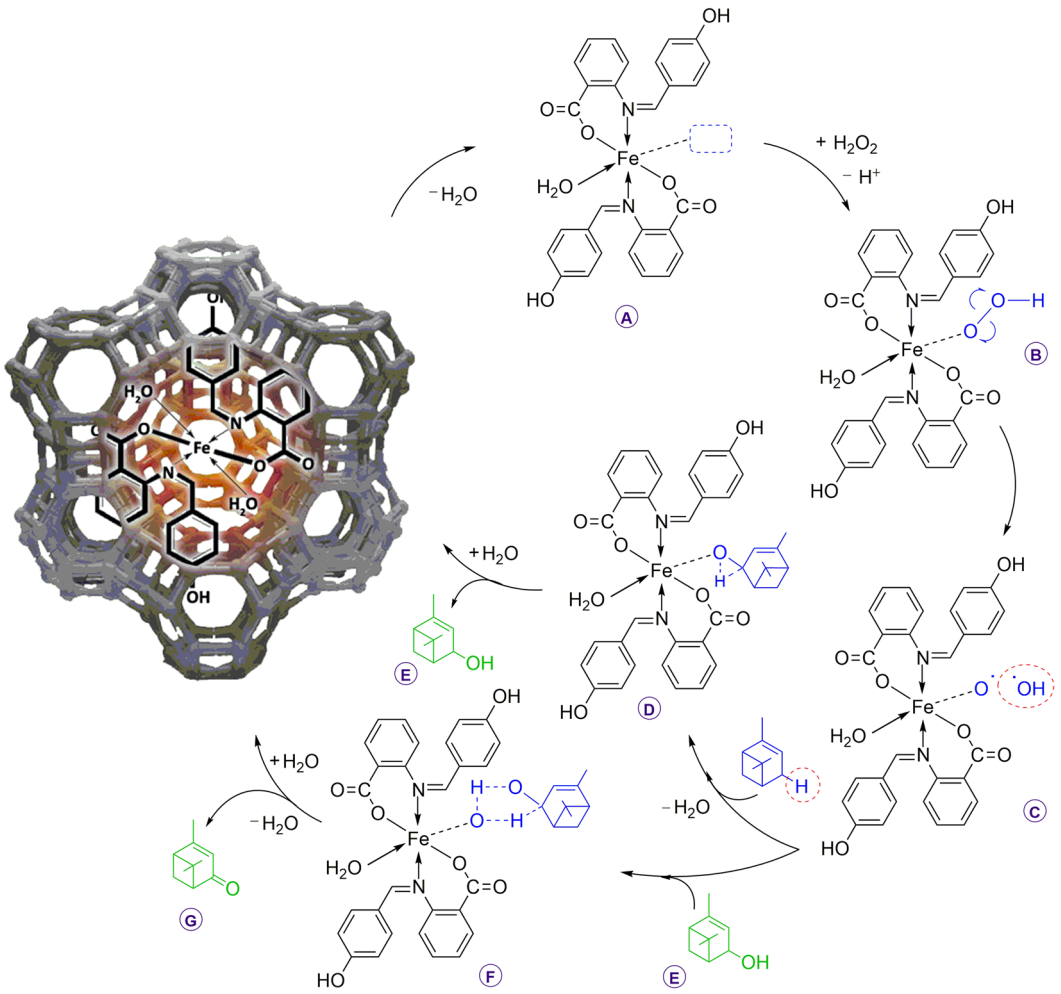

Scheme 4 The catalytic cycle for the oxidation of α-pinene using $[Fe(L)_2(H_2O)_2]$-Y catalyst with H_2O_2

reactivity, selectivity, stability, and lifetime of catalyst, which is unapproachable with homogeneous system.

Acknowledgements One of the authors, D.K. Parmar (JRF), is thankful to the University Grants Commission, New Delhi, India for providing financial support (F. No. 42–290/2013 (SR) dated 25/03/2013) to carry out this work.

References

1. L. Saikia, D. Srinivas, P. Ratnasamy, Appl. Catal. A: Gen. **309**, 144 (2006)
2. W.E. Erman, *An Encyclopedic Handbook* (Marcel Dekker, New York, 1985), p. 12
3. J.L.F. Monteiro, C.O. Veloso, Top. Catal. **27**, 180 (2004)
4. D. Clemente-Tejeda, A. López-Moreno, F.A. Bermejo, Tetrahedron **69**, 2977 (2013)
5. M. Ghorbanloo, A. Mohamadi, M. Amini, J. Tao, Trans. Met. Chem. **40**, 321 (2015)
6. L. Menini, M.J. da Silva, M.F.F. Lelis, J.D. Fabris, R.M. Lago, E.V. Gusevskaya, Appl. Catal. A: Gen. **269**, 117 (2004)
7. P. Oliveira, M.L. Rojas-Cervantes, A.M. Ramos, I.M. Fonseca, A.M. Botelho do Rego, J. Vital, Catal Today. **118**, 307 (2006)
8. E. Salminen, P. Mäki-Arvela, P. Virtanen, T. Salmi, J.P. Mikkola, Top Catal. **57**, 1533 (2014)
9. M. Tudorache, A. Gheorghe, A.S. Viana, V.I. Parvulescu, J. Mol. Catal. B: Enzym. **134**, 9 (2016)
10. D.R. Godhani, H.D. Nakum, D.K. Parmar, J.P. Mehta, N.C. Desai, Inorg. Chem. Commun. **72**, 105 (2016)
11. T. Joseph, D.P. Sawant, C.S. Gopinath, S.B. Halligudi, J. Mol. Catal. A: Chem. **184**, 289 (2002)
12. C.K. Modi, J.A. Chudasama, H.D. Nakum, D.K. Parmar, A.L. Patel, J. Mol. Catal. A: Chem. **395**, 151 (2014)
13. P.A.R. Dutenhefner, K.A. da Silva Rocha, E.M.B. Sousa, E.V. Gusevskaya, J. Catal. **265**, 72 (2009)
14. A. Wróblewska, Molecules. **19**, 19907 (2014)
15. S.M. Islam, A.S. Roy, P. Mondal, S. Paul, N. Salam, Inorg. Chem. Commun. **24**, 170 (2012)
16. K. Li, J. Valla, J. Garcia-Martinez, ChemCatChem **6**, 46 (2014)
17. N.V. Maksimchuk, M.N. Timofeeva, M.S. Melgunov, A.N. Shmakov, Y.A. Chesalov, D.N. Dybtsev, V.P. Fedin, O.A. Kholdeeva, J. Catal. **257**, 315 (2008)
18. J. Juan-Alcañiz, E.V. Ramos-Fernandez, U. Lafont, J. Gascon, F. Kapteijn, J. Catal. **269**, 229 (2010)
19. Y. Zhang, V. Degirmenci, C. Li, E.J.M. Hensen, ChemSusChem. **4**, 59 (2011)
20. O.V. Zalomaeva, K.A. Kovalenko, Y.A. Chesalov, M.S. Mel'gunov, V.I. Zaikovskii, V.V. Kaichev, A.B. Sorokin, O.A. Kholdeeva, V.P. Fedin, Dalton Trans. **40**, 1441 (2011)
21. E. Kockrick, T. Lescouet, E.V. Kudrik, A.B. Sorokin, D. Farrusseng, Chem. Commun. **47**, 1562 (2011)
22. K.K. Bania, D. Bharali, B. Viswanathan, R.C. Deka, Inorg. Chem. **51**, 1657 (2012)
23. K. Kervinen, P.C.A. Bruijnincx, A.M. Beale, J.G. Mesu, G. van Koten, R.J.M.K. Gebbink, B.M. Weckhuysen, J. Am. Chem. Soc. **128**, 3208 (2006)
24. A. Corma, H. Garcia, Eur. J. Inorg. Chem. **2004**(6) 1143–1164 (2004)
25. J.P. Mehta, D.K. Parmar, H.D. Nakum, D.R. Godhani, N.C. Desai, J. Porous Mater. **23**, 1507 (2016)
26. J.P. Mehta, D.K. Parmar, D.R. Godhani, H.D. Nakum, N.C. Desai, J. Mol. Catal. A: Chem. **421**, 178 (2016)
27. J.P. Mehta, D.K. Parmar, H.D. Nakum, D.R. Godhani, N.C. Desai, Microporous Mesoporous Mater. **247**, 198 (2017)
28. M.N. Ibrahim, S.A.I. Sharif, E- J. Chem. **8**, 180 (2011)
29. S. Koner, Chem. Commun. **5**, 593 (1998)
30. P. Chen, B. Fan, M. Song, C. Jin, J. Ma, R. Li, Catal. Commun. **7**, 969 (2006)
31. W.H. Quayle, J.H. Lunsford, Inorg. Chem. **21**, 97 (1982)
32. M. Jafarian, M. Rashvandavei, M. Khakali, F. Gobal, S. Rayati, M.G. Mahjani, J. Phys. Chem. C. **116**, 18518 (2012)
33. C.K. Modi, B.G. Gade, J.A. Chudasama, D.K. Parmar, H.D. Nakum, A.L. Patel, Spectrochim. Acta Mol. Biomol. Spectrosc. **140**, 174 (2015)
34. T. Mathur, J. Dinda, P. Datta, G. Mostafa, T.-H. Lu, C. Sinha, Polyhedron **25**, 2503 (2006)
35. T.K. Mondal, P. Raghavaiah, A.K. Patra, C. Sinha, Inorg. Chem. Commun. **13**, 273 (2010)
36. T.K. Mondal, J.-S. Wu, T.-H. Lu, R. Pallepogu, A.K. Patra, C. Sinha, Sk. Jasimuddin, J. Organomet. Chem. **694**, 3518 (2009)
37. T.K. Misra, D. Das, C. Sinha, P.K. Ghosh, C.K. Pal, Inorg. Chem. **37**, 1672 (1998)
38. F.A. Cotton, G. Wilkinson, C.A. Murillo, M. Bochmann, (1999) *Advanced Inorganic Chemistry* (Wiley, New York, pp. 1–1376)
39. B. Dutta, S. Jana, R. Bera, P.K. Saha, S. Koner, Appl. Catal. A: Gen. **318**, 89 (2007)
40. K. Balkus Jr., M. Eisa, R. Levedo, J. Am. Chem. Soc. **117**, 10753 (1995)
41. A. Corma, M.T. Nemeth, M. Renz, S. Valencia, Nature. **412**, 423 (2001)